coatings

MDPI

Article

Vibration Characteristics and Damping Analysis of the Blisk-Deposited Hard Coating Using the Rayleigh-Ritz Method

Feng Gao [1,2] and Wei Sun [1,2,*]

[1] School of Mechanical Engineering & Automation, Northeastern University, Shenyang 110819, China; peakgaoneu@163.com

[2] Key Laboratory of Vibration and Control of Aero-Propulsion System Ministry of Education, Northeastern University, Shenyang 110819, China

* Correspondence: weisun@mail.neu.edu.cn

Received: 15 June 2017; Accepted: 18 July 2017; Published: 25 July 2017

Abstract: For the purpose of improving the working reliability of the blisk (integrally-bladed disk) under severe environment, a passive vibration reduction method by depositing a hard coating on both sides of blades is developed and then investigated systematically. Firstly, an analytical model of the blisk-deposited hard coating is taken into account. Secondly, by using the Oberst beam theory and axial symmetry property, the composite hard-coated blade is equivalent to a special homogeneous blade possessing the equivalent material parameters. Then, energy equations of the blisk with hard-coated blades are derived by using the complex-valued modulus, and then substituted into the Lagrange equations. Additionally, eigenvalue equations of the blisk with hard-coated blades are acquired by taking advantage of Rayleigh-Ritz method, and its natural characteristics are obtained subsequently. Further, the frequency response functions of the blisk with hard-coated blades are formulated by using proportional damping to achieve its damping matrix. Finally, a stainless-steel blisk with deposited NiCoCrAlY + YSZ hard coating on both sides of the blades is chosen as the study case to conduct numerical calculations, and the results are compared with those obtained by experimental tests in terms of natural frequencies and mode shapes. The variation of natural frequencies, modal loss factors and frequency response functions of the blisk generated by hard coating are studied, respectively, and the influence of the coating thickness on the damping capacity are further discussed.

Keywords: blisk; hard coating; vibration characteristics; damping capacity; complex-valued modulus; Rayleigh-Ritz method

1. Introduction

Considerable attention has been paid to the blisk by researchers and used widely in the structural design of aero-engines. At present, a variety of alloy materials and process routes were applied to the blisk. On the basis of high-speed turning, milling, and grinding technologies, gamma titanium-aluminum alloys were widely chosen to produce blades of the blisk by Klocke et al. [1], Beranoagirre et al. [2,3], and Calleja et al. [4], and a five-axis machining process was utilized by Artetxe to manufacture the blisk [5]. Moreover, the blisk was applied to the F414-GE-400 engine installed in F/A-18E/F fighters, F119-PW-110 engine installed in F22 fighters, the WS500 engine installed in C602 cruise missiles, the EJ 200 HP compressor, and the 3E core engine [6,7]. Unlike the traditional bladed disk consisting of a single disk and some removable blades, it was manufactured as an integral whole without attached dovetails jointing the blade and disk. Thus, the number of components, mass, and abrasive wear of the blisk were effectively reduced, and the aerodynamic performance and

thrust-weight ratio were remarkably improved [8]. However, as a result of the absence of dovetail attachments providing structural damping, the blisk was easier to subject to coupling vibration between the blade and disk [9,10]. Consequently, the blisk was sensitive and vulnerable to severe resonant stress, which may give rise to high-cycle fatigue failure and lower the working reliability and safety of aero-engines [11,12]. It was estimated by the US Air Force that malfunctions caused by vibration failure of blades account for 70% in all the malfunctions of aero-engines [13]. Thus, it is vital to reduce the vibration of the blisk by using additional damping treatment. Generally, the shroud friction damper [14–16], under-platform damper [17–19], and friction ring damper [20–23] were widely used to conduct vibration reduction, however, all of them neglect the negative influence of high temperature and pressure on the brittle blades in harsh working conditions.

At present, hard coating, which possesses high hardness and better stability, was used mainly as a surface treatment to reinforce the surface performance of composite structures effectively, such as an anti-friction coating [24,25], thermal barrier coating [26,27] and anti-corrosive coating [28,29]. In 2000, Yen [30] found that the damping capacity and dynamic characteristics of vibrating structures can be improved by the energy dissipation due to internal particle friction. Subsequently, hard coating has been applied to the titanium plates [31–33], which were simplified as the blade, for vibration reduction. Moreover, the coating thickness is generally thinner than that of titanium plates; consequently, the resonant peaks can be suppressed without significantly altering the structural mass and stiffness of vibrating structures.

In order to fully consider the influence of structural damping (including hard-coating damping and substrate damping) on the composite structure, complex-valued modulus is widely utilized by researchers. Using the iterative complex-eigenvalue method and different constitutive models, Gounaris et al. [34] achieved the hysteretic damping of the composite structure in the resonant region. Rouleau et al. [35] dealt with the vibration reduction of a viscoelastic sandwich coupled to fluids, and calculated the response of a bi-dimensional sandwich ring. Natale et al. [36] conducted the complex modal analysis of rods equipped with an arbitrary number of viscous damping devices, and the influence of a variety of parameters on vibration results are discussed. In order to achieve the higher order theory of the sandwich beam, a viscoelastic beam with three layers was analyzed by Arikoglu and Ozkol [37] with a differential transform method in the frequency domain. Using an inverse method and a hard-coating cantilever beam, Sun et al. [38] successfully realized the identification of material parameters for hard-coating possessing a strain-dependence property. Moreover, creating the finite element model with the hard coating, Sun et al. [39] calculated the forced response of the hard-coating plate possessing the nonlinear dynamic characteristics, and compared with those obtained from the linear calculation and experiment, respectively.

The Rayleigh-Ritz method, most widely employed to solve structural vibration problems with variety of configurations and boundary conditions, is regarded as an efficient and effective numerical method for achieving an approximate and reliable solution. Using the Rayleigh-Ritz method and nonlocal elasticity theory, Chakraverty and Behera [40] conducted the free vibration analysis of the non-uniform Euler-Bernoulli nano-beams with boundary characteristic orthogonal polynomials, and found the relationship between frequency parameters. Applying the Rayleigh-Ritz method and shear deformation theory to the vibration analysis, Milazzo and Oliveri [41] captured the post-buckling behavior of the cracked composite plates and investigated the variation of natural characteristics generated by the large displacement. Making full use of the shear deformation theory and the Rayleigh-Ritz method, Wang and Wu [42] conducted the vibration analysis for a functionally-graded (FG) porous cylindrical shell, and achieved its natural characteristics in different sets of immovable boundary conditions. For a bladed disk with a coupling effect, artificial springs between the disk and blade were introduced at joints by Tomioka et al. [43], and the free vibration analysis was carried out by using the Rayleigh-Ritz method. For laminated cylindrical shells with arbitrary boundary conditions, Song et al. [44] conducted the traveling wave analysis accurately by using the Rayleigh-Ritz method and Donnel's shell theory. On the basis of the Rayleigh-Ritz assumed mode method, along with Kane's

method, rotating pre-twisted tapered blades made of functionally-graded materials are modeled with various dimensionless geometric parameters and analyzed to solve its vibration characteristics by Yutaek and Hong [45]. A coupled system with a pre-twisted blade attached to a rigid disk was modeled and investigated by Lee et al. [46] to capture its dynamic characteristics by taking advantage of Lagrange equation and Rayleigh-Ritz method.

The study described in this paper highlights the vibration reduction for the blisk by depositing a hard coating on the blades, and is organized as follows: In Section 2, the theoretical analysis of the blisk with hard-coated blades is conducted by using the complex-valued modulus theory together with the Rayleigh-Ritz method, such as the establishment of an analytical model, the derivation of the equivalent parameters for hard-coated blades, and the derivation of natural frequencies, loss factors, and frequency response functions. In Section 3, a stainless-steel blisk with a deposited NiCoCrAlY + YSZ hard coating on both sides of the blades is chosen to conduct numerical calculations, and the results are compared with those obtained by experimental testing. Moreover, the variation of natural frequencies, modal loss factors, and frequency response functions of the blisk, which are generated by NiCoCrAlY + YSZ hard-coating, are investigated, respectively, and the influence of the coating thickness on the damping capacity of the blisk are further discussed by both modal loss factors and frequency response functions.

2. Analytical Investigation of the Blisk with Hard-Coating Blades

2.1. Description for the Analytical Model

The analytical model of the blisk with hard-coating blades used for analytical analysis is shown in Figure 1. For the disk, its thickness is represented by h_d, r_i and r_o refer to its inner radius and outer radius respectively. By treating the center of the disk as the origin O_d, a cylindrical coordinate system (r, θ, x_1) is established, and the displacement of disk in the x_1 direction is denoted by u_d. Hard-coating blades are equispaced around the outer rim of the disk, its length and width are represented by l_b and w_b respectively, h_0 is delegated as its thickness including the thickness of blade h_b and hard coating 2 h_c, and ϕ refers to its stagger angle. Similarly, by treating the center of hard-coating blade as the origin O_{bj}, some local Cartesian coordinate systems (x_{1j}, x_{2j}, x_{3j}) (j = 1, 2, . . . , p is the number of hard-coating blades) are established, and the displacement of hard-coating blades in the x_{1j} direction is denoted by u_b.

It is noteworthy that the coupling effects between the hard-coated blades and disk exist, in fact, and are fully taken into consideration in the analytical analysis. Thus, a set of artificial springs possessing the rotational stiffness K_{Rj} and the translational stiffness K_{Tj} are introduced between hard-coating blades and the disk [47,48].

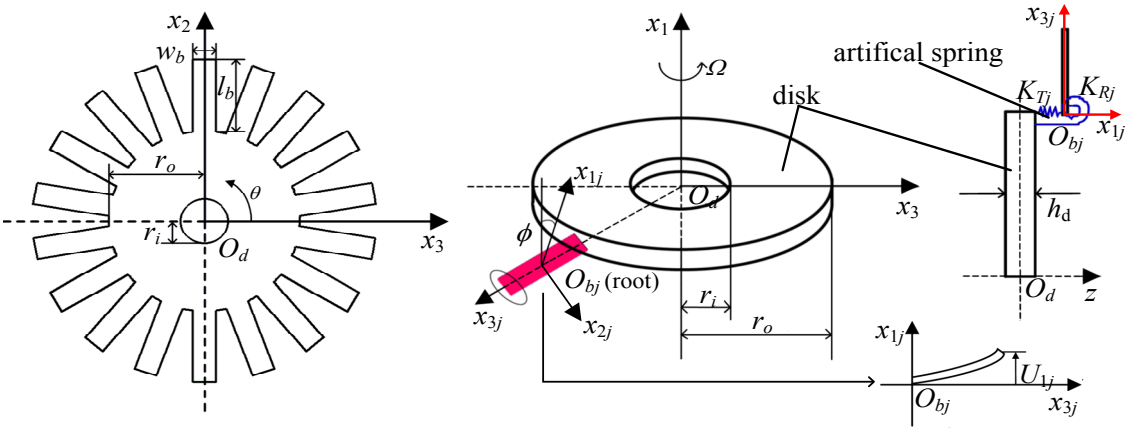

Figure 1. The analytical model of the blisk with hard-coating blades.

2.2. Solution for the Equivalent Parameters of Hard-Coated Blades

The hard-coated blade in the pure bending condition can be regarded as the composite Oberst beam, including the substrate beam and hard coating, as shown in Figure 2. Moreover, an effective and efficient approach that multilayer composites can be reduced as a single equivalent layer without increasing the number of active DOFs (degrees of freedom) of analytical model was proposed in [49]. Thus, using the axial symmetrical property, the equivalent material parameters of the hard-coating blade are derived.

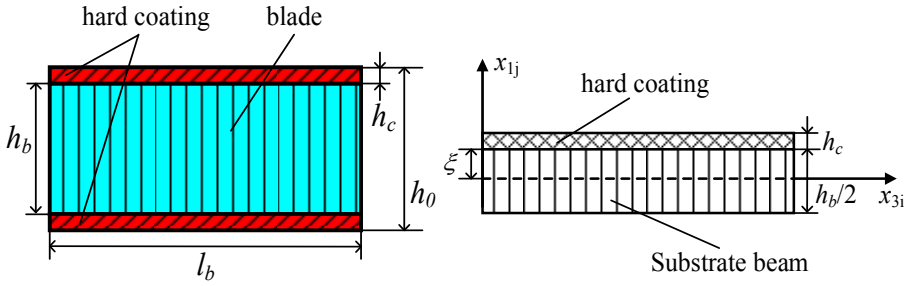

Figure 2. Schematic figure of the hard-coated beam.

E_b and E_c represent the Young's modulus of the substrate beam and hard coating, respectively, η_b and η_c refer to the loss factor of the substrate beam and hard coating, respectively. Thus, the complex-valued modulus of the substrate beam $\widetilde{E}_b$ and hard coating $\widetilde{E}_c$ can be written, respectively, as:

$$\widetilde{E}_b = E_b(1 + \mathrm{i}\eta_b),\ \widetilde{E}_c = E_c(1 + \mathrm{i}\eta_c),\ \mathrm{i} = \sqrt{-1} \tag{1}$$

Then, the equilibrium equation of the hard-coated beam can be expressed as:

$$\int_{\xi-\frac{h_b}{2}}^{\xi} E_b x_{1j} \mathrm{d}x_{1j} + \int_{\xi}^{\xi+\frac{h_b}{2}} E_c x_{1j} \mathrm{d}x_{1j} = 0 \tag{2}$$

where, ξ refers to the distance between the neutral surface and the interface of the hard-coating beam.

Further, the neutral surface of the hard-coated beam can be obtained from Equation (2) as:

$$\xi = \frac{E_b h_b^2 - 4E_c h_c^2}{4(E_b h_b + 2E_c h_c)} \tag{3}$$

Supposing $\widetilde{\omega}$ and $\widetilde{K}_{eb}$ as the transverse angular velocity and complex stiffness, respectively, the cross-sectional bending moment of the hard-coating beam $\widetilde{N}$ can be deduced as:

$$\begin{cases} \widetilde{N} = \widetilde{K}_{eb}\kappa = w_b\kappa \left(\int_{\xi-\frac{h_b}{2}}^{\xi} \widetilde{E}_b x_{1j}^2 \mathrm{d}x_{1j} + \int_{\xi}^{\xi+\frac{h_b}{2}} \widetilde{E}_c x_{1j}^2 \mathrm{d}x_{1j} \right) \\ \kappa = \frac{1}{\mathrm{i}\widetilde{\omega}} \frac{\partial \widetilde{\omega}}{\partial x_{1j}} \end{cases} \tag{4}$$

where, κ refers to the curvature of the hard-coated beam.

Then, the complex stiffness $\widetilde{K}_{eb}$ of the hard-coated beam can be acquired from Equation (4) as follows:

$$\widetilde{K}_{eb} = w_b \left(\int_{\xi-\frac{h_b}{2}}^{\xi} \widetilde{E}_b x_{1j}^2 \mathrm{d}x_{1j} + \int_{\xi}^{\xi+\frac{h_b}{2}} \widetilde{E}_c x_{1j}^2 \mathrm{d}x_{1j} \right) = \frac{w_b}{3} \left[\widetilde{E}_b \left(\frac{1}{8}h_b^3 - \frac{3}{4}h_b^2 + \frac{3}{2}h_b\xi^2 \right) + \widetilde{E}_c \left(h_c^3 + 3h_c^2 + 3h_c\xi^2 \right) \right] \tag{5}$$

Setting:

$$e = \frac{E_c}{E_b}, \widetilde{e} = \frac{\widetilde{E}_c}{\widetilde{E}_b}, \; h_{c/b} = \frac{h_c}{h_b} \tag{6}$$

Substituting Equation (3) into Equation (5), the complex stiffness $\widetilde{K}_{eb}$ of the hard-coated beam can be rewritten as:

$$\widetilde{K}_{eb} = \frac{1}{12}\widetilde{E}_b w_b h_b^3 \left(\frac{1 + 8\widetilde{e}h_{c/b} + 12\widetilde{e}h_{c/b}^2 + 16\widetilde{e}h_{c/b}^3 + 16\widetilde{e}^2 h_{c/b}^2}{1 + 2\widetilde{e}h_{c/b}} \right) \tag{7}$$

Correspondingly, the equivalent complex-valued modulus of the hard-coated beam $\widetilde{E}_{eb}$ can be derived as:

$$\begin{cases} \widetilde{E}_{eb} = E_{eb}(1 + \mathrm{i}\eta_{\mathrm{eb}}) \\ E_{eb} = \frac{1+8eh_{c/b}+12eh_{c/b}^2+16eh_{c/b}^3+16e^2h_{c/b}^4}{(1+2eh_{c/b})(1+2h_{c/b})}\mathrm{E}_b \\ \eta_{\mathrm{eb}} = \frac{2\left(3eh_{c/b}+12eh_{c/b}^2+16eh_{c/b}^3+16e^2h_{c/b}^4+16e^3h_{c/b}^5\right)}{(1+2eh_{c/b})\left(1+8eh_{c/b}+24eh_{c/b}^2+32eh_{c/b}^3+16e^2h_{c/b}^4\right)}(\eta_c - \eta_b) + \eta_b \end{cases} \tag{8}$$

where, E_{eb} and η_{eb} are the equivalent Young's modulus and loss factor of the hard-coated beam.

Moreover, the equivalent mass density of the hard-coating beam ρ_{eb} is deduced as:

$$\rho_{eb} = \frac{\rho_{bd}h_b + 2\rho_c h_c}{h_b + 2h_c} \tag{9}$$

where, ρ_{bd} and ρ_c refer to the mass density of the blisk and hard coating, respectively.

2.3. Solution for Energy Equations of Blisk with Hard-Coated Blades

The energy equations of the blisk with hard-coated blades which rotate at a constant speed ω are calculated, respectively. For the artificial springs simulating the coupling effects, its potential energy U_s are derived as:

$$U_s = \frac{1}{2}\sum_{j=1}^{p}\left[K_{Tj}\left(u_d - u_b\cos\phi_j\right)^2 + K_{Rj}\left(\frac{\partial u_d}{\partial r} - \frac{\partial u_b}{\partial x_{3j}}\cos\phi_j \right)^2 \right]_{|r=r_i,\theta=\theta_j,x_{3j}=0} \tag{10}$$

Supposing I_b as the cross-sectional inertia moment of the hard-coated blade, the strain energy U_b of the hard-coated blades can be derived as follows:

$$\begin{cases} U_b = \widetilde{E}_{eb} I_b \sum_{j=1}^{p} \int_0^{l_b} \left(\frac{\partial^2 u_b}{\partial x_{3j}^2} \right) \mathrm{d}x_{3j} \\ I_b = \frac{w_b(h_b+2h_c)^3}{12} \end{cases} \tag{11}$$

The kinetic energy T_b of the hard-coated blades is derived as follows:

$$\begin{cases} T_b = \frac{1}{2}\sum_{j=1}^{p} \rho_{eb} A_j \int_0^{l_b} \left(\frac{\partial u_b}{\partial t} \right)^2 \mathrm{d}x_{3j} \\ A_j = l_b w_b (h_b + 2h_c) \end{cases} \tag{12}$$

where, A_j refers to the volume of the hard-coated blade.

The potential energy V_b of the hard-coated blades is derived as follows:

$$V_b = \frac{\rho_{eb}\omega^2}{2}\sum_{j=1}^{p} A_j \left\{ \int_0^{l_b} \frac{\partial u_b}{\partial x_{3j}} \left[r_o\left(l_b - x_{3j}\right) + \frac{1}{2}\left(l_b^2 - x_{3j}^2\right) \right] - \left(u_b \sin\phi\right) \right\} \mathrm{d}x_{3j} \tag{13}$$

The strain energy U_d of the disk is deduced as follows:

$$\begin{cases} U_d = \frac{\widetilde{E}_d h_d^3}{24(1-\nu^2)} \int_{r_i}^{r_o} \int_0^{2\pi} \left\{ \begin{array}{c} \left(\frac{\partial^2 u_d}{\partial r^2} + \frac{1}{r}\frac{\partial u_d}{\partial r} + \frac{1}{r^2}\frac{\partial^2 u_d}{\partial \theta^2}\right)^2 - 2(1-\nu)\times \\ \left[\left(\frac{\partial^2 u_d}{\partial r^2}\right)\left(\frac{1}{r}\frac{\partial u_d}{\partial r} + \frac{1}{r^2}\frac{\partial^2 u_d}{\partial \theta^2}\right) - \left(\frac{\partial}{\partial r}\left(\frac{1}{r}\frac{\partial u_d}{\partial \theta}\right)\right)^2\right] \end{array} \right\} r \mathrm{d}\theta \mathrm{d}r \\ \widetilde{E}_d = \widetilde{E}_b \end{cases} \tag{14}$$

where, $\widetilde{E}_d$, h_d, and ν are the complex-valued modulus, thickness, and Poisson's ratio of the disk, respectively.

The kinetic energy T_d of the disk is deduced as follows:

$$T_d = \frac{1}{2}\rho_{bd} h_d \int_{r_i}^{r_o} \int_0^{2\pi} \left(\frac{u_d}{\partial t}\right)^2 r \mathrm{d}\theta \mathrm{d}r \tag{15}$$

The potential energy V_d of the disk is deduced as follows:

$$V_d = \frac{1}{2} h_d \int_{r_i}^{r_o} \int_0^{2} \left[\sigma_r \left(\frac{\partial u_d}{\partial r}\right)^2 + \sigma_\theta \left(\frac{1}{r}\frac{\partial u_d}{\partial \theta}\right)^2\right] r \mathrm{d}r \mathrm{d}\theta \tag{16}$$

where, σ_r and σ_θ are the radial and circumferential forces of the disk, respectively, and can be expressed as:

$$\begin{cases} \sigma_r = \frac{E_d}{1-\nu^2}\left(\nu\frac{u_{dr}}{r} + \frac{\mathrm{d}u_{dr}}{\mathrm{d}r}\right) \\ \sigma_\theta = \frac{E_d}{1-\nu^2}\left(\frac{u_{dr}}{r} + \nu\frac{\mathrm{d}u_{dr}}{\mathrm{d}r}\right) \end{cases} \tag{17}$$

where, u_{dr} refers to the displacement of the disk in the x_3 direction.

The radial equilibrium equation of the disk in the rotating state can be written as:

$$\frac{\mathrm{d}}{\mathrm{d}r}(h_d r \sigma_r) - h_d \sigma_\theta + h_d \rho_{bd} r^2 \omega^2 = 0 \tag{18}$$

Then, substituting Equation (17) into Equation (18), the radial equilibrium equation of the disk can be rewritten as:

$$r^2 \frac{\mathrm{d}^2 u_{dr}}{\mathrm{d}r^2} + r\frac{\mathrm{d}u_{dr}}{\mathrm{d}r} - u_{dr} = \left(\frac{\mathrm{E}_d}{1-\nu^2}\right)^{-1} \rho_{bd} r^3 \omega^2 \tag{19}$$

The general solution of Equation (19) with unknown coefficients Q_1 and Q_2 can be expressed as:

$$u_{dr} = Q_1 r + Q_2 r^{-1} - \frac{1-v^2}{8E_d}\rho_{bd}\omega^2 r^3 \tag{20}$$

The equilibrium equation of centrifugal force with different boundary conditions are derived, respectively, as:

$$\begin{cases} u_{dr} = 0, & r = r_i \\ 2\pi r_o h_d \sigma_r = \omega^2 \sum_{j=1}^{p} \rho_{bd} A_j l_b \left(r_o + \frac{l_b}{r_o}\right), & r = r_o \end{cases} \tag{21}$$

Substituting Equation (20) into Equation (21), the unknown coefficients Q_1 and Q_2 can be determined as:

$$\begin{cases} Q_1 = \frac{(1-\nu^2)\rho_{bd}\omega^2}{8E_d\left[(1-\nu)r_i^2+(1+\nu)r_o^2\right]}\left\{\left[(3+\nu)r_o^4+(1-\nu)r_i^4\right]+4r_o^2\left(r_o^2-r_i^2\right)Q_3\right\} \\ Q_2 = -\frac{(1-\nu^2)\rho_{bd}\omega^2 r_i^2 r_o^2}{8E_d\left[(1-\nu)r_i^2+(1+\nu)r_o^2\right]}\left\{\left[(3+\nu)r_o^4-(1+\nu)r_i^4\right]-4r_o^2\left(r_o^2-r_i^2\right)Q_3\right\} \\ Q_3 = \frac{\rho_{eb}}{2\pi\rho_{bd}h_d\left(r_o^2-r_i^2\right)r_o}\sum_{j=1}^{p}A_j\left(2r_o+l_b^2\right) \end{cases} \tag{22}$$

2.4. Solution for Orthogonal Polynomials of the Rayleigh-Ritz Method

For purpose of making free vibration analysis of the blisk with hard-coated blade simplification, several non-dimensional parameters are derived as follows:

$$a = \frac{r}{r_o}, b = \frac{x_{3j}}{l_b}, c = \frac{r_i}{r_o} \tag{23}$$

On the basis of the supposition principle of small deformation theory, the displacement of hard-coated blades u_b and disk u_d with frequency ω are expressed, respectively, as [50]:

$$\begin{cases} u_b\left(x_{3j},t\right) = r_o U_b(b)\sin(\omega t) \\ u_d(r,\theta,t) = r_o U_d(a,\theta)\sin(\omega t) \end{cases} \tag{24}$$

where, $U_b(b)$ and $U_d(a,\theta)$ refer to the mode shapes of the hard-coated blades and the disk, respectively, and can be written, respectively, with unknown coefficients B_{r_b}, A_{mn}^c, and A_{mn}^s as:

$$\begin{cases} U_b(b) = \sum_{r_b=1}^{R_b} B_{r_b}\psi_{r_b}(b) \\ U_d(a,\theta) = \sum_{m=1}^{M}\sum_{n=0}^{N}\Phi_m(a)\left[A_{mn}^c\cos(n\theta)+A_{mn}^s\sin(n\theta)\right] \end{cases} \tag{25}$$

where, B_{r_b} and M refer to the number of Ritz polynomial dimensions of the hard-coated blades and disk, respectively; N is the number of nodal diameters of the blisk with hard-coated blades; and $\psi_{r_b}(b)$ and $\Phi_m(a)$, employed as the admissible functions, are the orthogonal polynomials of the hard-coated blades and disk, respectively, and derived by the Gram-Schmidt process with respect to the recurrence formula:

$$\begin{cases} F_2(x) = (x-B_2)F_1(x) \\ F_\alpha(x) = (x-B_\alpha)F_{\alpha-1}(x) - C_\alpha F_{\alpha-2}(x) \\ B_\alpha = \frac{\int xf(x)F_{\alpha-1}^2\mathrm{d}x}{\int f(x)F_{\alpha-1}^2\mathrm{d}x}, C_\alpha = \frac{\int f(x)F_{\alpha-1}^2\mathrm{d}x}{\int f(x)F_{\alpha-2}^2\mathrm{d}x} \\ \alpha \geq 3 \end{cases} \tag{26}$$

where, $F_\alpha(x)$ and $f(x)$ refer to the polynomials and weighting function, respectively.

For the hard-coated blades:

$$F_\alpha(x) \equiv \Phi_m(a), f(x) \equiv a, \alpha \equiv m, x \equiv a \tag{27}$$

For the disk:

$$F_\alpha(x) \equiv \psi_{r_b}(b), f(x) \equiv 1, \alpha \equiv r_b, x \equiv b \tag{28}$$

Then, the integrations of the hard-coated blades and disk are implemented, respectively, with respect to $c \le a \le 1$ and $0 \le b \le 1$. Supposing $G_{\alpha\beta}$ as the non-zero values, the polynomials of the hard-coated blades and disk are satisfied with the following orthogonality condition together, i.e.,

$$\int f(x)F_\alpha(x)F_\beta(x)\mathrm{d}x = \begin{cases} 0 & \alpha \neq \beta \\ G_{\alpha\beta} & \alpha = \beta \end{cases} \tag{29}$$

and the starting expressions which are applied to hard-coating blades and disk can be written, respectively, as:

$$\psi_1(b) = 1, \Phi_1(a) = (a-c)^2 \tag{30}$$

2.5. Vibration Characteristics of the Blisk with Hard-Coated Blades

Substituting Equations (10)–(16) into the Lagrange equation:

$$L = T_b + T_d - (V_b + V_d + U_b + U_d + U_s) \tag{31}$$

On basis of the minimal potential principle, together with Equations (26)–(30), the eigenvalue equation of the blisk with hard-coated blades can be derived as:

$$\left(\widetilde{\mathbf{K}} - \widetilde{\lambda}^2\mathbf{M}\right)\mathbf{X} = \mathbf{0} \tag{32}$$

where, $\widetilde{\mathbf{K}}$ and $\widetilde{\lambda}$ refer to the complex stiffness matrix and complex eigenvalues respectively, $\boldsymbol{M}$ and $\boldsymbol{X}$ refers to the mass matrix and eigenvectors, respectively:

$$\begin{cases} \widetilde{\mathbf{K}} = \begin{bmatrix} \mathbf{K}_{mn}^{cc} & \mathbf{K}_{mn}^{sc} & -\mathbf{K}_{r_b}^{c} \\ \mathbf{K}_{mn}^{cs} & \mathbf{K}_{mn}^{ss} & -\mathbf{K}_{r_b}^{s} \\ -\mathbf{K}_{mn}^{cb} & -\mathbf{K}_{mn}^{sb} & \mathbf{K}_{r_b} \end{bmatrix} \\ \mathbf{M} = \begin{bmatrix} \mathbf{M}_{mn}^{c} & \mathbf{0} & \mathbf{0} \\ \mathbf{0} & \mathbf{M}_{mn}^{s} & \mathbf{0} \\ \mathbf{0} & \mathbf{0} & \mathbf{M}_{r_b} \end{bmatrix} \\ \mathbf{X} = \begin{bmatrix} \mathbf{A}_{mn}^{c} & \mathbf{A}_{mn}^{s} & \mathbf{B}_{r_b} \end{bmatrix}^T \end{cases} \tag{33}$$

where $\mathbf{K}_{mn}^{cc}$ and $\mathbf{K}_{mn}^{ss}$ are related to the symmetric mode and the antisymmetric mode of the disk, respectively; $\mathbf{K}_{mn}^{sc}$ and $\mathbf{K}_{mn}^{cs}$ reflect the coupling effect between the symmetric mode and the antisymmetric mode of the disk together; $\mathbf{K}_{r_b}^{c}$, $\mathbf{K}_{r_b}^{s}$, $\mathbf{K}_{mn}^{cb}$, and $\mathbf{K}_{mn}^{sb}$ reflect the influence of the symmetric and the antisymmetric modes of the disk on the hard-coated blades together; and $\mathbf{A}_{mn}^{c}$, $\mathbf{A}_{mn}^{s}$ and $\mathbf{B}_{r_b}$ are diagonal submatrices. Then, the natural frequencies f_γ and modal loss factor η_γ of the blisk with hard-coated blades are deduced, respectively, as below [51]:

$$f_\gamma = \frac{\omega_\gamma}{2\pi} = \frac{\sqrt{\mathrm{Re}\left(\widetilde{\lambda}_\gamma\right)}}{2\pi}, \eta_\gamma = \frac{\mathrm{Im}\left(\widetilde{\lambda}_\gamma\right)}{\mathrm{Re}\left(\widetilde{\lambda}_\gamma\right)} \tag{34}$$

where, γ refers to the mode index, $\mathrm{Re}\left(\widetilde{\lambda}_\gamma\right)$ and $\mathrm{Im}\left(\widetilde{\lambda}_\gamma\right)$ refer to the real part and imaginary part of the complex eigenvalues, respectively. It is very difficult to calculate the damping matrix directly, especially for the composite structures. Thus, the proportional damping [52], which can be implemented efficiently by using the mass and stiffness matrices, combined with the proportional constants μ and τ, is utilized to obtain the damping matrix $\boldsymbol{D}$ of the blisk with hard-coated blades with the following formulas:

$$\mathbf{D} = \mu\mathbf{M} + \tau\mathbf{K}, \mu + \tau\omega_\gamma = \eta_\gamma\omega_\gamma \tag{35}$$

Finally, the frequency response function of the simple blisk with hard-coated blades can be achieved:

$$H(\omega) = \sum_{\gamma=1} \frac{\mathbf{X}_\gamma \mathbf{X}_\gamma^T}{\omega_\gamma^2 - \omega^2 + i\omega D_\gamma} \tag{36}$$

3. Numerical Results and Its Discussion

3.1. Description of the Blisk and Experimental Devices

The stainless-steel blisk with cyclic symmetry property and experimental procedure are shown in Figure 3. The devices mainly include a mode hammer providing the impulsive excitation, and a specific fixture fixing the blisk, a B&K-4517 lightweight acceleration transducer (B&K, Skodsborgvej, Denmark) delivering the response signal, an LMS mobile SCADAC front-end (LMS, Rouwen, Belgium) (sixteen channel data acquisition controller), and a mobile workstation with LMS Test.lab (Rel. 12.0, LMS) installed. Moreover, by taking advantage of the APS (air plasma spraying) technique, NiCoCrAlY + YSZ hard coating is deposited on both sides of all the blades with a coating thickness of 0.15 mm, as shown in Figure 4.

The nominal geometric parameters of the blisk are listed in Table 1, and the nominal mechanical parameters of the blisk and hard coating, which was obtained from the mechanical design handbook (in Chinese) and DMA (dynamic thermomechanical analysis), are listed, respectively, in Table 2.

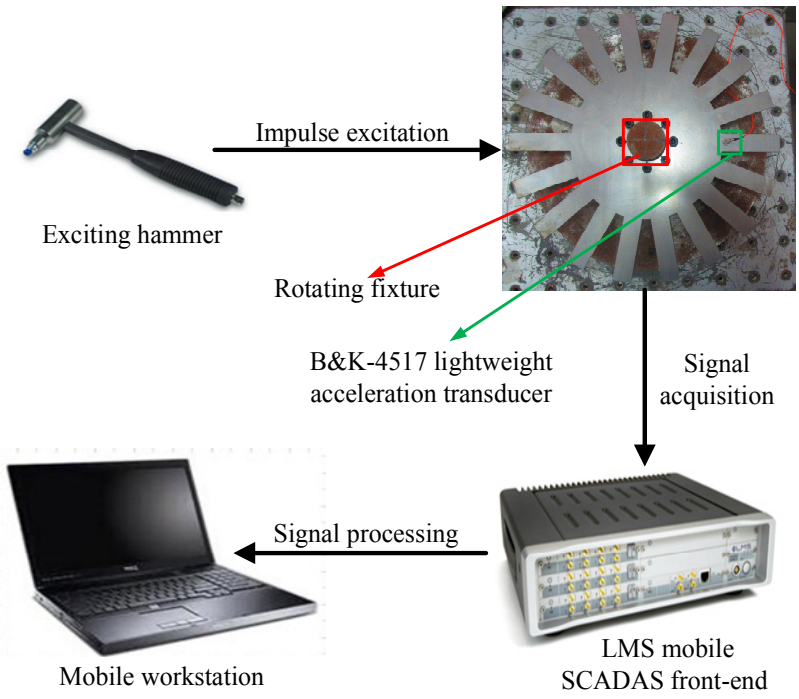

Figure 3. The stainless-steel blisk and experimental devices.

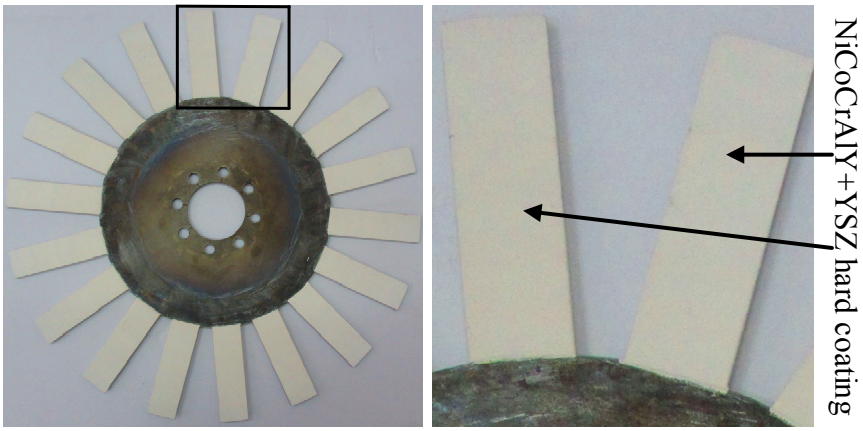

Figure 4. The blisk with the deposited NiCoCrAlY + YSZ hard coating on its blades.

Table 1. Geometry parameters of the blisk with hard-coating blades.

Catalog	Disk	Blade	Hard Coating
Length or Outer radius (mm)	100	80	80
Width or Inner radius (mm)	25	24	24
Thickness (mm)	3	3	0.15
Number	1	18	18

Table 2. Material parameters of the blisk with hard-coated blades.

Catalog	Disk	Blade	Hard Coating
Material	Q235-A(F) steel	Q235-A(F) steel	NiCoCrAlY + YSZ
Young's modulus (Gpa)	208	208	54.494
Mass density (kg/m^3)	7860	7860	5600
Poisson's ratio	0.277	0.277	0.30
Loss factor	0.0004	0.0004	0.0212

3.2. Numerical Results and Experimental Verification

Supposing the K_{Tj} and K_{Rj} as 10^8 N/m, both natural frequencies and mode shapes of the blisk with hard-coating blades are achieved, respectively, by the Rayleigh-Ritz method. In contrast, a hammer-peening experiment is carried out to verify the accuracy of results each other. Firstly, multiple measured points of the blisk model, which was established in the Geometry module of the LMS Test.lab, were peened orderly by the exciting hammer, and then the response signals of the SB blisk were transferred to the LMS front-end SCADAC by making use of the lightweight B&K-4517 acceleration transducer (about 0.16 g) fixed on the root of one conventional blade. Further, data analysis to obtain natural frequencies and mode shapes was accomplished in the PolyMAX module of LMS Test.lab. By analyzing the stabilization diagram of frequency response functions obtained from the above mentioned experimental test, natural frequencies and mode shapes of the blisk with hard-coating blades are extracted from the PolyMAX module of LMS Test.lab, respectively. The stabilization diagrams of the blisk with hard-coated blades within 1500 Hz are shown in Figure 5.

Natural frequencies obtained by Rayleigh-Ritz method and experimental test and its comparison are listed in Table 3. The results obtained by two ways are different due to the imperfection of the experimental test, but the difference of the same-order results are very small, within 5%. Additionally, the consistency of results shows that the modes ranging from first-order to eighth-order are, generally, dense.

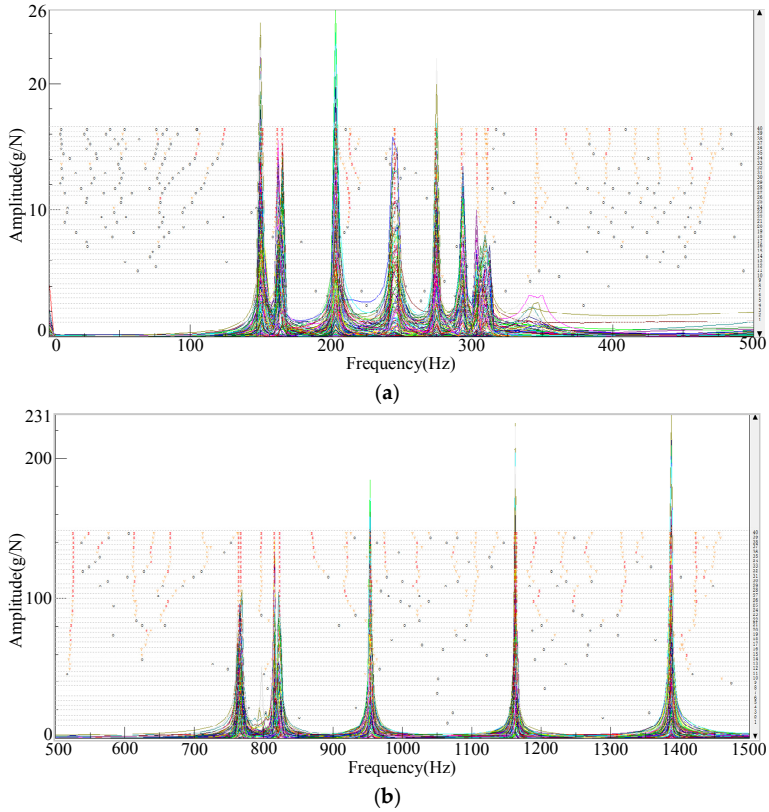

Figure 5. Stabilization diagrams within 1500 Hz. (**a**) Stabilization diagram ranging from 0 to 500 Hz; and (**b**) the stabilization diagram ranging from 500 to 1500 Hz.

Table 3. Natural frequencies obtained by the Rayleigh-Ritz method and experimental testing (Hz).

Mode Order	Rayleigh-Ritz Method	Experimental Test	Difference
1	147.66	150.39	1.82%
2	161.05	165.71	2.81%
3	208.66	203.87	−2.35%
4	250.95	245.34	−2.29%
5	282.65	274.45	−2.99%
6	301.97	292.89	−3.10%
7	321.32	308.45	−4.17%
8	340.13	345.85	1.65%
9	735.48	764.80	3.83%
10	795.25	821.07	3.14%
11	939.63	953.98	1.50%
12	1205.01	1164.13	−3.51%
13	1408.70	1387.74	−1.51%

Figure 6 displays the mode shapes of the first- and second-order when n = 3, obtained by the Rayleigh-Ritz method and experimental testing. In the analytical analysis, the results of the blisk with hard-coating blades are represented by the mode shapes of the disk and a representative blade together. The blue and green distributions indicate the location possessing small vibration amplitude (even nearly zero), the yellow and red distributions indicate the location possessing large vibration amplitudes. It is revealed that the coupling vibrations between the disk and hard-coating blade dominate the structural vibrations. Moreover, it is found that a nodal circle appears on the circumferential blades and the disk in the second-order mode. In the experimental test, the yellow and red distributions indicate the small-amplitude zone and large-amplitude zone, respectively. On the whole, the results obtained by two methods show good consistency.

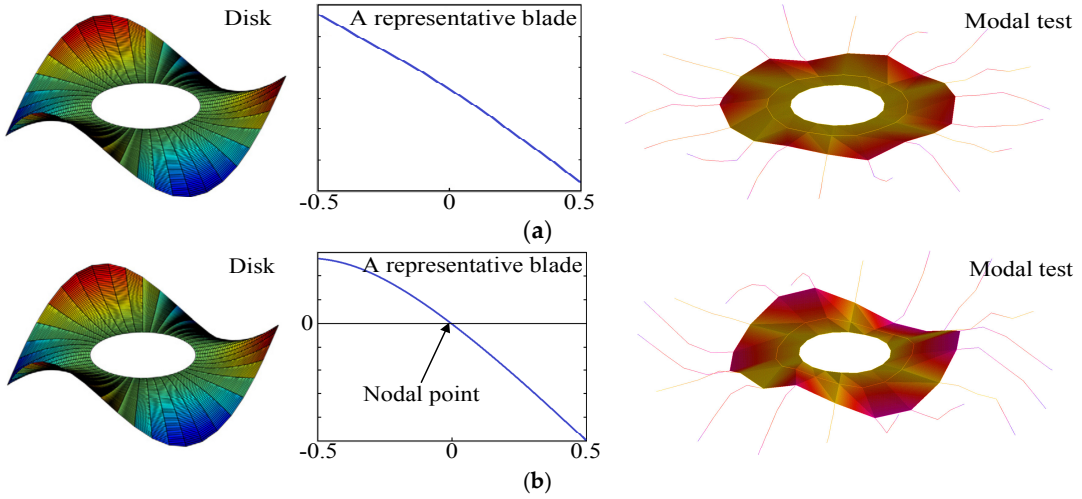

Figure 6. Mode shapes obtained by the Rayleigh-Ritz method and experimental test. (**a**) The first-order mode shapes when n = 3; and (**b**) The second-order mode shapes when n = 3.

3.3. The Influence of Hard Coating on Vibration Characteristics

Generally, hard coating plays an important role in the dynamical behavior of the composite structure, and its influence on vibration characteristics of the blisk is essential and necessary to be investigated in this paper. Table 4 lists natural frequencies of the blisk with or without hard coating obtained by Rayleigh-Ritz method and experimental test. The comparison of results is carried out for the purpose of studying the variation tendency of natural frequencies brought about by NiCoCrAlY + YSZ hard coating. It can be seen clearly that natural frequencies decrease generally than ever, but the change gradients are confined within 4% for Rayleigh-Ritz method and within 5% for the experimental test.

Table 4. Natural frequencies of the blisk with or without hard coating (Hz).

Mode Order	Rayleigh-Ritz Method			Experimental Test		
	Blisk	Hard-Coating Blisk	Change Gradient	Blisk	Hard-Coating Blisk	Change Gradient
1	148.57	147.66	−0.62%	152.58	150.39	−1.46%
2	162.78	161.05	−1.07%	168.86	165.71	−1.90%
3	212.71	208.66	−1.94%	210.46	203.87	−3.23%
4	254.90	250.95	−1.57%	255.41	245.34	−4.10%
5	289.39	282.65	−2.38%	281.38	274.45	−2.53%
6	312.25	301.97	−3.40%	305.64	292.89	−4.35%
7	327.94	321.32	−2.06%	320.72	308.45	−3.98%
8	346.91	340.13	−1.99%	357.28	345.85	−3.30%
9	754.21	735.48	−2.55%	792.19	764.8	−3.58%
10	825.07	795.25	−3.75%	860.71	821.07	−4.83%
11	963.57	939.63	−2.55%	984.50	953.98	−3.20%
12	1246.17	1205.01	−3.42%	1211.64	1164.13	−4.08%
13	1464.58	1408.70	−3.97%	1450.02	1387.74	−4.49%

Modal loss factors of the blisk, with or without hard-coating, obtained by the Rayleigh-Ritz method and experimental test are plotted in Figure 7. It is known that the damping theory for composite structures is imperfect, and the experimental environment is complicated and changeable. Thus, the modal loss factors are achieved with an unavoidable error, M1 $\neq$ M2 and M3 $\neq$ M4. However, the variation tendencies of results obtained by two ways are always similar in general. Moreover, modal loss factors increase significantly by eight times, approximately, which is different from the natural frequencies.

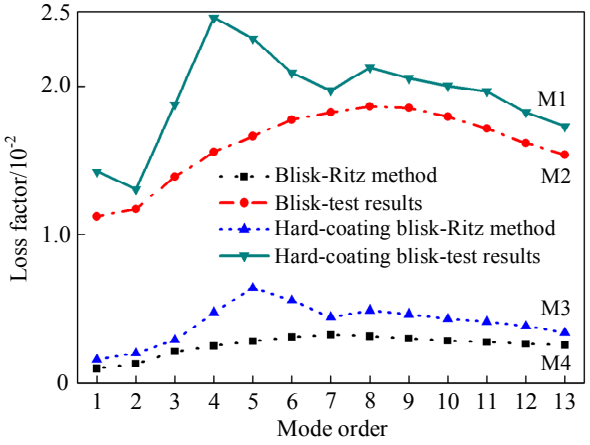

Figure 7. Modal loss factors of the blisk with or without hard-coating.

The frequency response functions of the blisk, with or without hard-coating, within 6000 Hz are plotted clearly in Figure 8. It can be seen explicitly that the amplitude at resonant frequencies are suppressed remarkably by the NiCoCrAlY + YSZ hard coating. Additionally, the declining gradient of the amplitude is increasingly apparent, especially for the high-order modes.

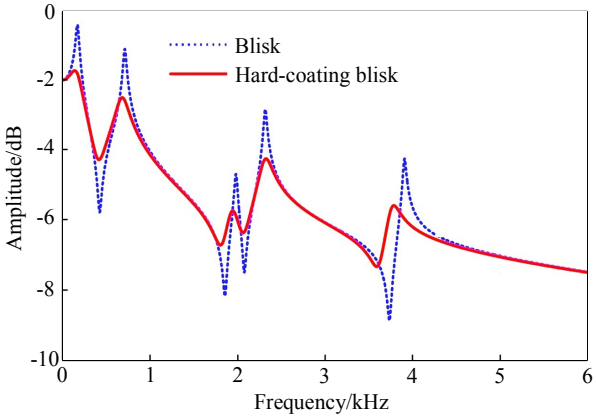

Figure 8. Frequency response functions of the blisk, with or without hard-coating.

3.4. The Influence of Coating Thickness on Damping Capacity

The emphasis on vibration reduction for the blisk is the improvement of damping capacity, and the damping capacity variation can be implemented efficiently by adjusting the coating thickness in actual applications. Thus, the influence of coating thickness on damping capacity is studied in terms of modal loss factors and frequency response functions.

Figure 9 illustrates the variation trends of modal loss factors of the blisk with different coating thicknesses ranging from 0 to 0.25 mm. It is revealed explicitly that the modal loss factors of the blisk increase as the coating thickness increases. However, the increased gradients of modal loss factors reduce gradually, and it can be found that the increased gradients alert slightly at $h_c > 0.15$ mm or $h_{c/b} > 5\%$.

The frequency response functions of the blisk with different coating thickness ranging from 0.15 mm to 0.25 mm are illustrated in Figure 10. Results reveal that the amplitudes of the blisk at resonant frequencies decline as the coating thickness increases. However, the decreased gradients of the amplitudes diminish gradually. Particularly, the decreased gradients are not obvious at $h_c > 0.15$ mm, which is in accordance with the variation trends of modal loss factors.

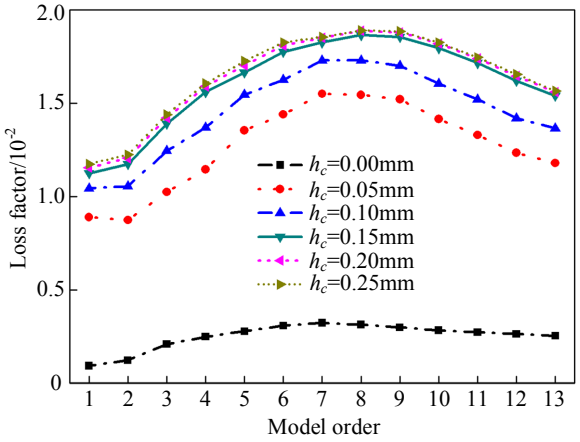

Figure 9. Modal loss factors of the blisk with different coating thicknesses.

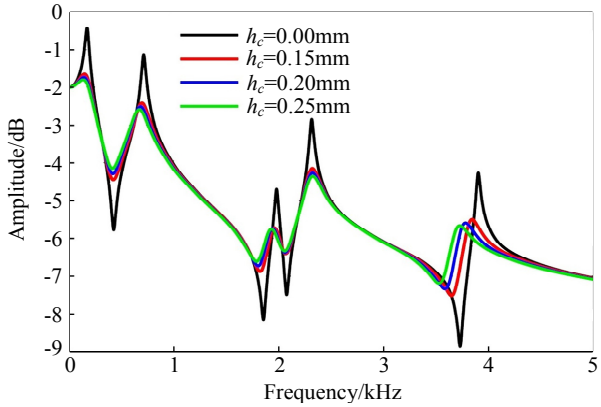

Figure 10. Frequency response functions of the blisk with different coating thicknesses.

4. Conclusions

A passive method for vibration reduction of the blisk by depositing a hard coating on both sides of the blades is developed in conditions of high temperature and pressure. On the basis of the established constitutive mode of the blisk with hard-coating blades, vibration characteristics of the composite structure are calculated, respectively, by utilizing the complex-valued modulus and Rayleigh-Ritz method, and compared with experimental results for verifying the validation of the analytical method.

Natural frequencies, loss factors, and frequency response functions of the blisk with hard-coated blades are obtained by the Rayleigh-Ritz method and experimental testing, respectively. A comparison of the results is carried out to investigate the influence of NiCoCrAlY + YSZ hard coating on the blisk. The results reveal clearly that NiCoCrAlY + YSZ hard coating has a small effect on the natural frequencies, but a good damping effect on the blisk, and the resonant response of the blisk at resonant frequencies is suppressed remarkably by the NiCoCrAlY + YSZ hard coating.

The influence of the coating thickness on the damping capacity of the blisk, with an emphasis on loss factors and frequency response functions, are further deduced and discussed because of its flexibility in actual application. It can be found explicitly that modal loss factors increase as the hard coating thickens, but its increased gradients reduce gradually. When $h_c > 0.15$ mm or $h_{c/b} > 5\%$, the increase of modal loss factors becomes smaller and smaller, and the decreased gradients of amplitudes are no longer obvious.

With the continuous development of new technologies and materials, hard coatings are the future evolution of damping treatments. Not only will APS and PVD be investigated, but also thermal spray

coatings, for vibration reduction, such as single-coating (NiCrAlY, YSZ, Y_2O_3, and CeO_2, etc.) and composite coatings with different bond layers of MgO + Al_2O_3 and NiCoCrAlY + Al_2O_3, etc. Moreover, more complicated and complex structures will be selected as study cass to study the damping strategy of hard coating for the next future.

Acknowledgments: This project is supported by the National Natural Science Foundation of China (Grant No. 51375079) and the Fundamental Research Funds for the Central Universities of China (Grant No. N150304008).

Author Contributions: Feng Gao conceived, designed and performed the experiments, analyzed the data and wrote the paper; Wei sun contributed materials, analysis tools and financial support.

Conflicts of Interest: The authors declare no conflict of interest.

References

1. Klocke, F.; Lung, D.; Arft, M.; Priarone, P.C.; Settineri, L. On high-speed turning of a third-generation gamma titanium aluminide. *Int. J. Adv. Manuf. Technol.* **2013**, *65*, 155–163. [CrossRef]
2. Beranoagirre, A.; Olvera, D.; de Lacalle, L.N.L. Milling of gamma titanium-aluminum alloys. *Int. J. Adv. Manuf. Technol.* **2012**, *62*, 83–88. [CrossRef]
3. Beranoagirre, A.; de Lacalle, L.N.L. Grinding of gamma TiAl intermetallic alloys. *Procedia Eng.* **2013**, *63*, 489–498. [CrossRef]
4. Calleja, A.; Fernández, A.; Rodríguez, A.; de Lacalle, L.N.L.; Lamikiz, A. Turn-milling of blades in turning centres and multitasking machines controlling tool tilt angle. *Proc. Inst. Mech. Eng. Part B J. Eng. Manuf.* **2015**, *229*, 1324–1336. [CrossRef]
5. Artetxe, E.; González, H.; Calleja, A.; Valdivielso, A.F.; Polvorosa, R.; Lamikiz, A.; de Lacalle, L.N.L. Optimised methodology for aircraft engine IBRs five-axis machining process. *Int. J. Mechatron. Manuf. Syst.* **2016**, *9*, 385–401. [CrossRef]
6. Kosing, O.E.; Scharl, R.; Schmuhl, H.J. Design Improvements of the EJ 200 HP Compressor: From Design Verification Engine to a Future All Blisk Version. In Proceedings of the ASME Turbo Expo 2001 Power for Land, Sea, and Air, New Orleans, LA, USA, 4–7 June 2001; American Society of Mechanical Engineers: New York, NY, USA, 2001.
7. Klinger, H.; Lazik, W.; Wunderlich, T. The engine 3E core engine. In Proceedings of the ASME Turbo Expo 2008: Power for Land, Sea, and Air, Berlin, Germany, 9–13 June 2008; American Society of Mechanical Engineers: New York, NY, USA, 2008; pp. 93–102.
8. Younossi, O.; Arena, M.V.; Moore, R.M.; Lorell, M.; Mason, J. *Military jet Engine Acquisition: Technology Basics and Cost-Estimating Methodology*; RAND Corp.: Santa Monica, CA, USA, 2002.
9. Klauke, T.; Kühhorn, A.; Beirow, B.; Golze, M. Numerical investigations of localized vibrations of mistuned blade integrated disks (blisks). *J. Turbo-Mach.* **2009**, *131*, 031002. [CrossRef]
10. Sever, I.A.; Petrov, E.P.; Ewins, D.J. Experimental and numerical investigation of rotating bladed disk forced response using underplatform friction dampers. *J. Eng. Gas Turbines Power* **2008**, *130*, 042503. [CrossRef]
11. Mbaye, M.; Soize, C.; Ousty, J.P.; Capiez-Lernout, E. Robust analysis of design in vibration of turbomachines. *J. Turbomach.* **2013**, *135*, 021008. [CrossRef]
12. Mayorca, M.A.; Fransson, T.H.; Mårtensson, H. A new reduced order modeling for stability and forced response analysis of aero-coupled blades considering various mode families. *J. Turbomach.* **2012**, *134*, 051008. [CrossRef]
13. Sinha, A. Computation of the statistics of forced response of a mistuned bladed disk assembly via polynomial chaos. *J. Vib. Acoust.* **2006**, *128*, 449–457. [CrossRef]
14. Sayed, B.A.; Chatelet, E.; Baguet, S.; Jacquet-Richardet, G. Dissipated energy and boundary condition effects associated to dry friction on the dynamics of vibrating structures. *Mech. Mach. Theory* **2011**, *46*, 479–491. [CrossRef]
15. Zhao, P.F.; Zhang, Q.; Wu, J.; Zhang, D. Experimental study of dynamic characteristics of dry friction damping of turbine blade steel. *Adv. Mater. Res.* **2013**, *690*, 1979–1982. [CrossRef]

16. Li, G.; Zhang, Q.; Zhao, W.; Zhou, Q.; Xie, Y.H. Dynamic response analysis of blades with damping structures of shroud and snubber. In Proceedings of the First International Conference on Information Sciences, Machinery, Materials and Energy, Jinan, China, 15–16 October 2015; Atlantis Press: Amsterdam, The Netherlands, 2015.
17. Sanliturk, K.Y.; Ewins, D.J.; Stanbridge, A.B. Underplatform dampers for turbine blades: Theoretical modelling, analysis and comparison with experimental data. *J. Eng. Gas Turbines Power* **2001**, *123*, 919–929. [CrossRef]
18. Petrov, E.P.; Ewins, D.J. Advanced modeling of underplatform friction dampers for analysis of bladed disk vibration. *J. Turbomach.* **2007**, *129*, 143–150. [CrossRef]
19. Pesaresi, L.; Salles, L.; Jones, A.; Green, J.S.; Schwingshackl, C.W. Modelling the nonlinear behaviour of an underplatform damper test rig for turbine applications. *Mech. Syst. Signal Process.* **2017**, *85*, 662–679. [CrossRef]
20. Laxalde, D.; Thouverez, F.; Sinou, J.; Lombard, J.P. Qualitative analysis of forced response of blisks with friction ring dampers. *Eur. J. Mech.-A/Solids* **2007**, *26*, 676–687. [CrossRef]
21. Laxalde, D.; Thouverez, F.; Lombard, J.P. Vibration control for integrally bladed disks using friction ring dampers. In Proceedings of the ASME Turbo Expo 2007: Power for Land, Sea, and Air, Montreal, QC, Canada, 14–17 May 2007; American Society of Mechanical Engineers: New York, NY, USA, 2007; pp. 255–265.
22. Laxalde, D.; Gibert, C.; Thouverez, F. Experimental and numerical investigations of friction rings damping of blisks. In Proceedings of the ASME Turbo Expo 2008: Power for Land, Sea, and Air, Berlin, Germany, 9–13 June 2008; American Society of Mechanical Engineers: New York, NY, USA, 2008; pp. 469–479.
23. Laxalde, D.; Thouverez, F.; Lombard, J.P. Forced response analysis of integrally bladed disks with friction ring dampers. *J. Vib. Acoust.* **2010**, *132*, 011013. [CrossRef]
24. Wei, S.B.; Pei, X.H.; Shi, B.R.; Shao, T.M.; Li, T.; Li, Y.L.; Xie, Y. Wear resistance and anti-friction of expansion cone with hard coating. *Pet. Explor. Dev.* **2016**, *43*, 326–331. [CrossRef]
25. Shubin, A.Y.; Potekaev, A.I.; Savostikov, V.M.; Galsanov, S.V.; Dmitriev, V.S.; Stepanov, I.B.; Kashkarov, E.B.; Dammer, V.H. Comparative physical-tribological properties of anti-friction ion-plasma Ti-C-Mo-S coating on VT6 alloy or 20X13 and 40X steels. In Proceedings of the IOP Conference Series: Materials Science and Engineering, Bangkok, Thailand, 20–21 April 2017; IOP Publishing: Bristol, UK, 2017.
26. Stathopoulos, V.; Sadykov, V.; Pavlova, S.; Bespalko, Y.; Fedorova, Y.; Bobrova, L.; Salanov, A.; Ishchenko, A.; Stoyanovsky, V.; Larina, T. Design of functionally graded multilayer thermal barrier coatings for gas turbine application. *Surf. Coat. Technol.* **2016**, *295*, 20–28. [CrossRef]
27. Zhu, W.; Wang, J.W.; Yang, L.; Zhou, Y.C.; Wei, Y.G.; Wu, R.T. Modeling and simulation of the temperature and stress fields in a 3D turbine blade coated with thermal barrier coatings. *Surf. Coat. Technol.* **2017**, *315*, 443–453. [CrossRef]
28. Wojciechowski, J.; Szubert, K.; Peipmann, R.; Fritz, M.; Schmidt, U.; Bund, A.; Lota, G. Anti-corrosive properties of silane coatings deposited on anodised aluminium. *Electrochim. Acta* **2016**, *220*, 1–10. [CrossRef]
29. Gao, Y.; Syed, J.A.; Lu, H.; Meng, X.K. Anti-corrosive performance of electropolymerized phosphomolybdic acid doped PANI coating on 304SS. *Appl. Surf. Sci.* **2016**, *360*, 389–397. [CrossRef]
30. Yen, H.Y. New Analysis and Design Procedures for Ensuring Gas Turbine Blades and Adhesive Bonded Joints Structural Integrity and Durability. Ph.D. Thesis, Ohio State University, Columbus, OH, USA, 2000.
31. Li, H.; Ying, L.; Sun, W. Analysis of nonlinear vibration of hard coating thin plate by finite element iteration method. *Shock Vib.* **2014**, *2014*. [CrossRef]
32. Yang, Z.X.; Han, Q.K.; Jin, Z.H.; Qu, T. Solution of natural characteristics of a hard-coating plate based on Lindstedt-Poincaré perturbation method and its valedictions by FEM and measurement. *Nonlinear Dyn.* **2015**, *81*, 1207–1218. [CrossRef]
33. Torvik, P.J.; Langley, B. Material properties of hard coatings developed for high damping. In Proceedings of the 51st AIAA/SAE/ASEE Joint Propulsion Conference, Orlando, FL, USA, 27–29 July 2015.
34. Gounaris, G.D.; Antonakakis, E.; Papadopoulos, C.A. Hysteretic damping of structures vibrating at resonance: An iterative complex eigensolution method based on damping-stress relation. *Comput. Struct.* **2007**, *85*, 1858–1868. [CrossRef]
35. Rouleau, L.; Deü, J.F.; Legay, A.; Sigrist, J.F. Vibro-acoustic study of a viscoelastic sandwich ring immersed in water. *J. Sound Vib.* **2012**, *331*, 522–539. [CrossRef]

36. Alati, N.; Failla, G.; Santini, A. Complex modal analysis of rods with viscous damping devices. *J. Sound Vib.* **2014**, *333*, 2130–2163. [CrossRef]
37. Arikoglu, A.; Ozkol, I. Vibration analysis of composite sandwich beams with viscoelastic core by using differential transform method. *Compos. Struct.* **2010**, *92*, 3031–3039. [CrossRef]
38. Sun, W.; Li, H.; Han, Q. Identification of mechanical parameters of hard-coating materials with strain-dependence. *J. Mech. Sci. Technol.* **2014**, *28*, 81. [CrossRef]
39. Sun, W.; Liu, Y.; Du, G. Analytical modeling of hard-coating cantilever composite plate considering the material nonlinearity of hard coating. *Math. Probl. Eng.* **2015**, *2015*. [CrossRef]
40. Chakraverty, S.; Behera, L. Free vibration of non-uniform nanobeams using Rayleigh-Ritz method. *Phys. E Low-Dimens. Syst. Nanostruct.* **2015**, *67*, 38–46. [CrossRef]
41. Milazzo, A.; Oliveri, V. Post-buckling analysis of cracked multilayered composite plates by pb-2 Rayleigh-Ritz method. *Compos. Struct.* **2015**, *132*, 75–86. [CrossRef]
42. Wang, Y.; Wu, D. Free vibration of functionally graded porous cylindrical shell using a sinusoidal shear deformation theory. *Aerosp. Sci. Technol.* **2017**, *66*, 83–91. [CrossRef]
43. Tomioka, T.; Kobayashi, Y.; Yamada, G. Analysis of free vibration of rotating disk-blade coupled systems by using artificial springs and orthogonal polynomials. *J. Sound Vib.* **1996**, *191*, 53–73. [CrossRef]
44. Song, X.; Zhai, J.; Chen, Y.; Han, Q.K. Traveling wave analysis of rotating cross-ply laminated cylindrical shells with arbitrary boundaries conditions via Rayleigh-Ritz method. *Compos. Struct.* **2015**, *133*, 1101–1115. [CrossRef]
45. Oh, Y.; Yoo, H.H. Vibration analysis of rotating pretwisted tapered blades made of functionally graded materials. *Int. J. Mech. Sci.* **2016**, *119*, 68–79. [CrossRef]
46. Lee, H.; Song, J.S.; Cha, S.J.; Na, S. Dynamic response of coupled shaft torsion and blade bending in rotor blade system. *J. Mech. Sci. Technol.* **2013**, *27*, 2585–2597. [CrossRef]
47. Xie, K.; Chen, M.; Zhang, L.; Xie, D. Wave based method for vibration analysis of elastically coupled annular plate and cylindrical shell structures. *Appl. Acoust.* **2017**, *123*, 107–122. [CrossRef]
48. Chen, Y.; Zhai, J.; Han, Q. Vibration and damping analysis of the bladed disk with damping hard coating on blades. *Aerosp. Sci. Technol.* **2016**, *58*, 248–257. [CrossRef]
49. Sanliturk, K.Y.; Koruk, H. Development and validation of a composite finite element with damping capability. *Compos. Struct.* **2013**, *97*, 136–146. [CrossRef]
50. Sun, S.; Cao, D.; Han, Q. Vibration studies of rotating cylindrical shells with arbitrary edges using characteristic orthogonal polynomials in the Rayleigh-Ritz method. *Int. J. Mech. Sci.* **2013**, *68*, 180–189. [CrossRef]
51. Jin, G.; Yang, C.; Liu, Z. Vibration and damping analysis of sandwich viscoelastic-core beam using Reddy's higher-order theory. *Compos. Struct.* **2016**, *140*, 390–409. [CrossRef]
52. Yoon, Y.C.; Kim, K.H.; Lee, S.H. Dynamic particle difference method for the analysis of proportionally damped system and cracked concrete beam. *Int. J. Fract.* **2016**, *23*, 1–26. [CrossRef]